Materials Transactions, Vol. 45, No. 1 (2004) pp. 65 to 68
Special Issue on Application of Nano-Structures Formed under Irradiation of Higher Energy Particles

Plane and Cross-Sectional TEM Observation to Clarify the Effect of Damage Region by Ion Implantation on Induced Phase Transformation in Austenitic 301 Stainless Steel

Dwi Gustiono*, Norihito Sakaguchi, Tamaki Shibayama, Hiroshi Kinoshita and Heishichiro Takahashi

Center for Advanced Research of Energy Technology, Hokkaido University, Sapporo 060-8628, Japan

Phase transformation in austenitic 301 stainless steel was studied under 300 keV Fe^+ and Ar^+ ions implantations to fluence of 1×10^{21} ions m^{-2} at room temperature, in order to pursuit the nucleation of martensitic phase transformation in ion-implanted region. Microstructures after ion implantation were observed by transmission electron microscopy (TEM) with plane view and for cross-sectional specimens. The plane view observation of the implanted specimen showed that phase transformation from the γ phase to α phase was induced due to implantation to doses of 5×10^{20} Fe^+ ions m^{-2} and 1×10^{20} Ar^+ ions m^{-2}. The nucleation of implantation-induced phase increased with increasing of fluence. The orientation relationship between the γ matrix and the induced α phase was identified to be $(1\bar{1}0)_\alpha \parallel (11\bar{1})_\gamma$ and $[111]_\alpha \parallel [011]_\gamma$, close to the Kurdjumov-Sachs (K-S) for the Fe^+ ion implanted specimen, and $(110)_\alpha \parallel (11\bar{1})_\gamma$ and $[001]_\alpha \parallel [0\bar{1}1]_\gamma$ close to the Nishiyama-Wasserman (N-W) for the Ar^+ ion implanted specimen. The cross-sectional observation after implantation revealed that the phase transformation preferentially nucleated in the region near the surface in metal (Fe^+) ion implanted specimen, because the gradient of implanted ion concentration attains maximal near the surface. On the other hand, the behavior of phase transformation in the Ar^+ ion implanted specimen was different from that of Fe^+ ion implantation and the phase was induced at deeper region from surface than Fe^+ ion case.

(Received August 11, 2003; Accepted December 18, 2003)

Keywords: *stainless steel, phase transformation, induced phase, ion implantation, cross-sectional observation*

1. Introduction

It is well known that martensitic phase transformation is often caused in austenitic stainless steels under stress. According to Schaeffler phase-diagram, the stability of the austenitic phase depends on the alloy compositions. This phase transformation from a γ (fcc) phase to an α (bcc) phase in austenitic stainless steel can be induced by cold-working and hydrogen charging treatments.[1–9)]

It has been reported that ion implantation or irradiation also induce phase transformation in metals and alloys,[10–22)] namely ion implantation at alloy constituent elements, and inert gas ions into austenitic stainless steel takes place the phase transformation from the γ phase to the α phase.[13–24)]

Microstructural observations using a transmission electron microscopy (TEM) have revealed that ion implantation into austenite stainless steel introduces microstructural change[14–17)] so that the transformed phase with various size from 10 to 200 nm in diameter[16–18)] is formed near the ion-implanted surface, and the fraction and size of the phase increased with dose of ion implantation.[15,17,19)] The induced α phase transformation in austenitic stainless steel is independent from that implanted ion species such as austenite stabilizer element (Ni), ferrite stabilizer element (Cr) and inert gas (Ar).[18)] It has been also confirmed that the relationship between γ matrix and the induced α phase is close to the relation of Nishiyama-Wasserman[25)] than that of Kurdjumov-Sach.[26)]

Furthermore, it has been suggested that the martensite transformation is associated with the stress concentration[18–21)] induced by the distribution of implanted ions. However, the actual mechanism and more detailed microstructures related to phase transformation under ion implantation are still not clear.

In this paper, plane and cross sectional TEM observations were performed for type 301 austenitic stainless steel after ion implantation of Fe^+ and Ar^+ ions. Clarification to the microstructures related to phase transformation under ion implantation was examined.

2. Experimental Procedures

Commercial grade austenitic 301 stainless steel disk of 3 mm in diameter were cut from the sheet with 0.15 mm thick, and annealed at 1373 K for 1.8 ks. The foils for transmission electron microscopy (TEM) were prepared by electro-polishing using a twin jet equipment in a solution of 95% acetic acid and 5% perchloric acid at 289 K. Specimens for cross-sectional observation were prepared using focused ion beam (FIB) instrument operated using 30 keV Ga^+ ions.

The ion implantation was carried out with 300 keV Fe^+ and Ar^+ ions at room temperature using an ion accelerator. The specimens were implanted to dose levels of 5×10^{20} Fe^+ m^{-2}, 1×10^{20} and 5×10^{20} Ar^+ m^{-2}. The projected ranges of 300 keV Fe^+ and Ar^+ ions in austenitic 301 stainless steel calculated with TRIM code are 200 and 300 nm, respectively. TEM observations were performed by JEOL JEM-2000FX and JEOL JEM-2010F operated at 200 kV.

3. Results and Discussions

In a specimen implanted to a dose of 5×10^{20} Fe^+ ions m^{-2} at room temperature, a lot of precipitate images and damage structures were observed in the γ matrix. These precipitates were also observed in a specimen after implan-

*Corresponding author, E-mail: gustiono@ufml.caret.hokudai.ac.jp

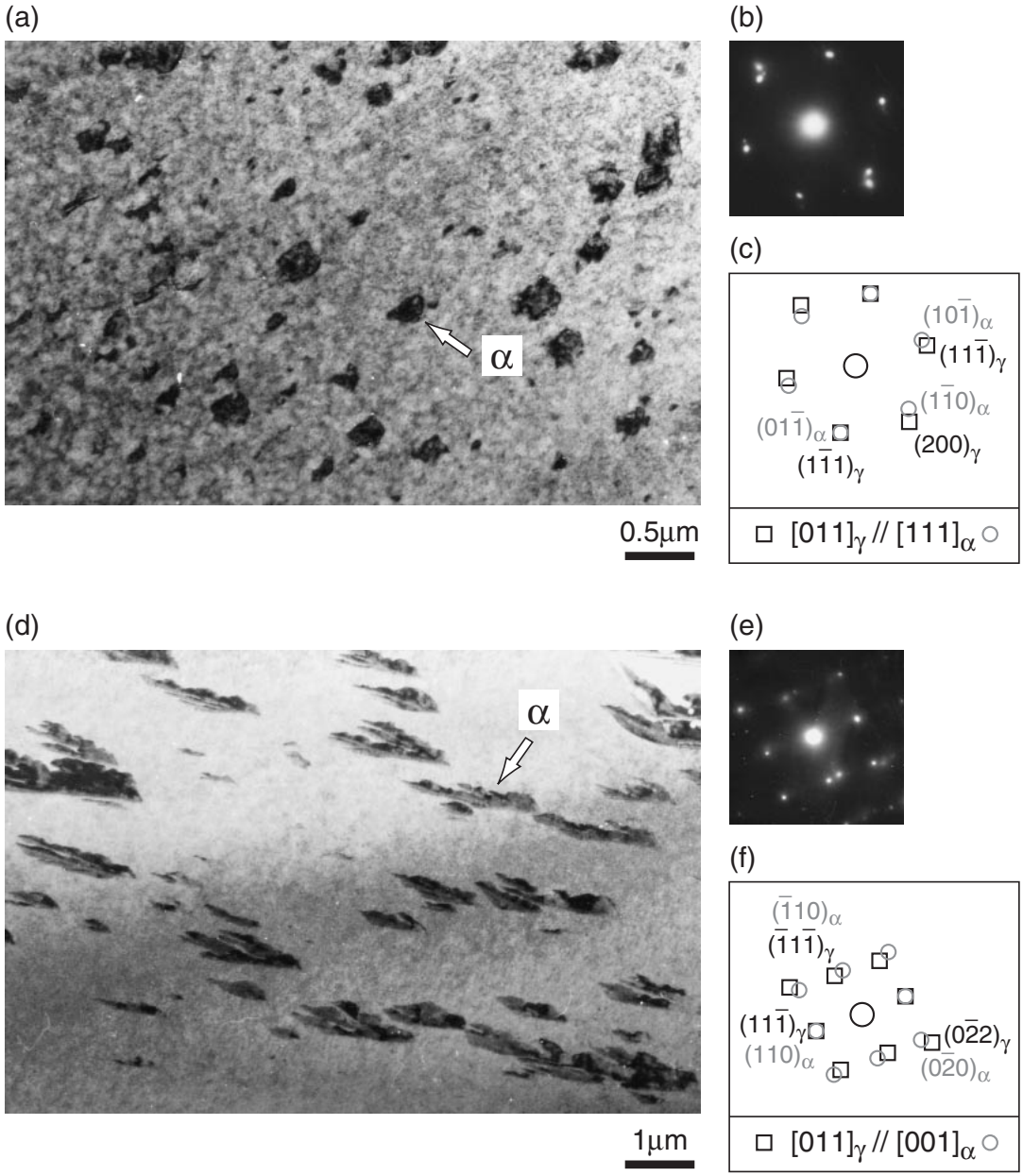

Fig. 1 TEM micrographs and schematic representations of SAD pattern in type 301 austenitic stainless steel specimens implanted to fluences of 5×10^{20} Fe ions m^{-2} (a-c) and 1×10^{20} Ar ions m^{-2} (d-f) at room temperature. (a) and (d) BF images, (b) and (e) SAD patterns of the γ matrix and the induced α phase, (c) and (f) schematic representation of the SAD patterns.

tation to a dose of 1×10^{20} Ar^+ ions m^{-2}. The number density of the precipitates increased with increasing of implantation dose.

Figure 1 shows a transmission electron micrograph of the austenitic 301 stainless steel implanted with 300 keV Fe^+ and Ar^+ ions to doses of 5×10^{20} ions m^{-2} and 1×10^{20} ions m^{-2}, respectively, at room temperature. Figures 1(a) and (d) are the microstructures observed from near $[001]_\gamma$ beam direction. The diffraction patterns obtained from γ matrix and the precipitates were given in Figs. 1(b) and 1(e). The implantation-induced precipitates were identified as α phase from the diffraction patterns, where incident directions are $[011]_\gamma$ and $[111]_\alpha$ for the austenite matrix and the induced α phase due to the Fe^+ ion implantation, respectively. On the other hand, for the case of Ar^+ ion implantation, the direction of incident electron beam for the matrix and the α phase correspond $[011]_\gamma$ and $[001]_\alpha$, respectively. Figs. 1(c) and 1(f) indicate indexes of the obtained diffractions for matrix and the α phase induced due to implantation of Ar^+ and Fe^+ ions. The analysis of these diffraction spots showed parallel relations of the $(01\bar{1})_\alpha \parallel (1\bar{1}1)_\gamma$ and $(\bar{1}\bar{1}0)_\alpha \parallel (\bar{1}\bar{1}1)_\gamma$ in the cases of Fe^+ ion and Ar^+ ion implantations, respectively. Thus, it is suggested that the orientation relation between γ matrix and the induced α phase due to Fe^+ ion implantation are $[111]_\alpha \parallel [011]_\gamma$ and $(01\bar{1})_\alpha \parallel (1\bar{1}1)_\gamma$, which closely correspond to the orientation relations of Kurdjumov-Sachs (K-S). Also the orientation relation for Ar^+ ion implantation are $[001]_\alpha \parallel [011]_\gamma$ and $(110)_\alpha \parallel (11\bar{1})_\gamma$ which are close to the orientation relationships of Nishiyama-Wassermann (N-W).

The size of the induced phase due to Ar^+ ion implantation is larger and its shape is different from that in Fe^+ ion

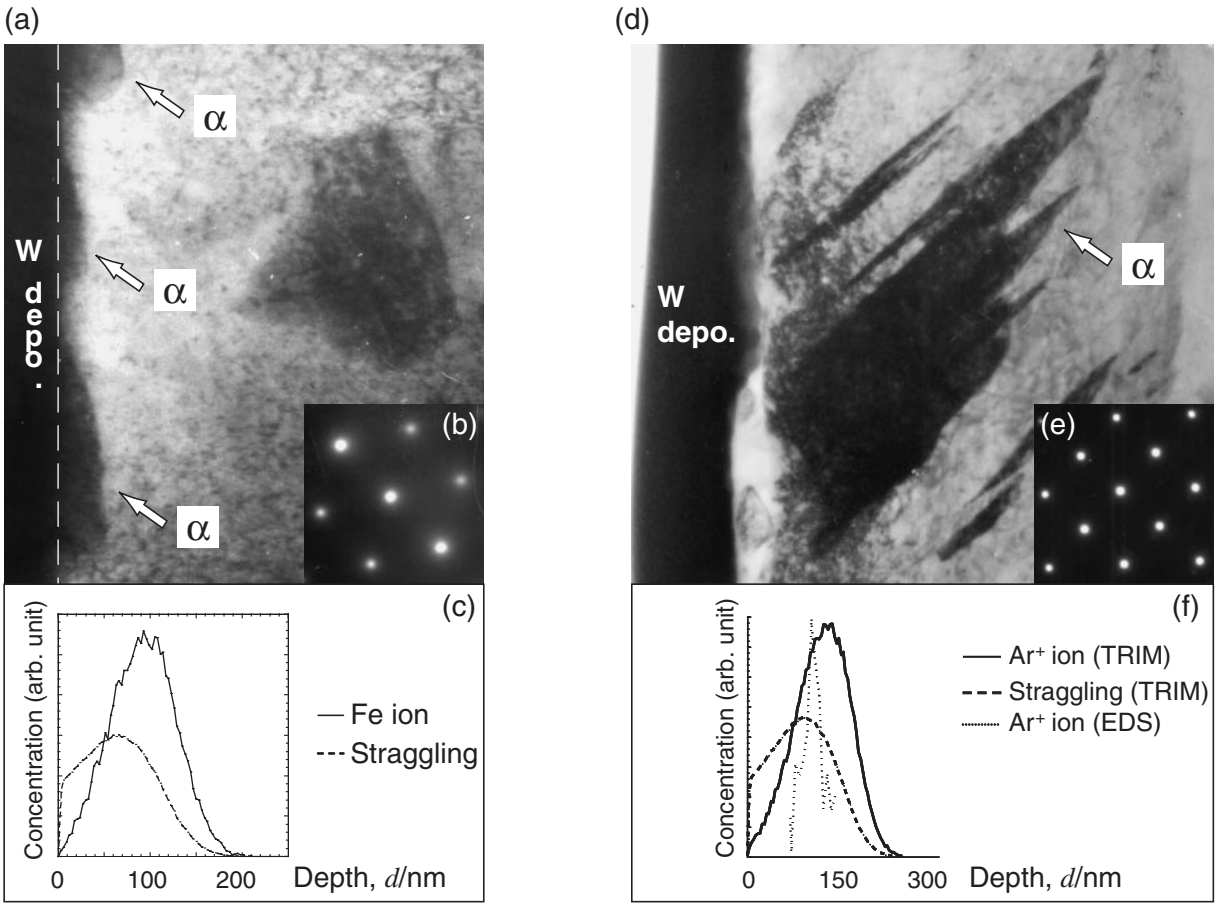

Fig. 2 TEM micrographs of cross-sectional specimens implanted to fluences of 5×10^{20} Fe ions m^{-2} (a-c) and 5×10^{20} Ar ions m^{-2} (d-f) at room temperature. (a) and (c) BF images, (b) and (e) SAD patterns of the induced α phase, (c) and (f) distribution profiles of both ions and damages to the depth according to TRIM code and EDS analysis.

implanted specimen. It is well known that ion implantation of inert gas into austenite stainless steel produce bubbles including the gases, as being revealed in 304 stainless steel when Ne^+ ions were implanted at the temperature below 425 K.[24] The bubble formation is not directly observed in the austenitic stainless steels in the process of implantation of gas ions.[18,20,22] It is suggested that local stress due to the bubble formation and/or clusters of the implanted gas atoms might affect martensitic phase transformation. Therefore, the local stress introduced by a distribution of implant gas seems to influence in wider range than that of the Fe^+ ion implantation.

Figure 2 shows TEM bright field images for the cross sectional view of the specimen implanted with 300 keV Fe^+ and Ar^+ ions to fluence of 5×10^{20} ions m^{-2} at room temperature. Concentration profiles of the implanted ions and the damage distributions calculated by TRIM-code were also displayed in the figure. The α phases observed from $[111]_\alpha$ and $[001]_\alpha$ directions were shown in Figs. 2(a) and (d). The dark field image contrast near surface indicated by arrow (the dark contrast along outer surface is W coating layer coated for the protection of surface layer from the damage during FIB fabrication) corresponded to α phase. Figures. 2(c) and (f) shows the depth profiles of the Fe and Ar stainless steel after implantation at 300 keV, respectively. The peak concentrations of the implanted Fe^+ and Ar^+ ions are at about 100 nm and 150 nm in depth away from the surface (calculated with TRIM code), respectively. The damage peak is at about 60 nm for Fe^+ ion and 110 nm for Ar^+ ion in depth. From the cross-sectional observation, it is indicated that most of α phases induced by Fe^+ implantation were nucleated near the surface in the ion implanted region. Thus, with comparing the microstructures and the profiles of the range and the straggling of ions (see Fig. 2(a)), the nucleation position of the α phase is not coincident with the range of peak damage and/or peak concentration of implanted elements. These facts suggest that the implantation-induced phase transformation is not directly related to concentration of implanted ions and the introduced damage defects during implantation near surface region away from the damage and the concentration peaks, namely the most of the phase transformation might be preferentially caused in the region corresponding to the highest concentration gradient in ion implanted depth profile in which the local stress concentration may be introduced. From the stress distribution estimated for the Fe^+ ion concentration profile, it is suggested that the position of strain field expected from the concentration gradient was about 30 nm in depth from specimen surface, which corresponded to the distribution region of the observed phases. Furthermore, the phase transformation may be enhanced the internal stress introduced by the irradiation damage due to implantation as being

seen in the Ar^+ ion implanted specimen. Also a segregation effect of the implanted ion species on the phase transformation should be considered but implantation temperature in this experiment is at room temperature, so the effect is seemed to be negligible.

4. Conclusions

From present experiment on ion implantation induced martensitic phase transformation in 301 stainless steel using an ion accelerator, following results are summarized;

(1) The phase transformation from γ (fcc) phase to α (bcc) phase was observed in thin film specimens of type 301 austenitic stainless steel implanted with 300 keV Fe^+ and Ar^+ ions at room temperature. The number density and the mean size of the α phase increased with dose of ion implantation.

(2) The orientation-relationships between the induced α phase and the γ phase for the Fe^+ ion implanted specimen was close to that of Kurdjumov-Sachs relationship ($(1\bar{1}0)_\alpha \parallel (11\bar{1})_\gamma$ and $[111]_\alpha \parallel [011]_\gamma$). The martensitic phase induced due to Ar^+ ions showed the relation of Nishiyama-Wassermann relationship ($(110)_\alpha \parallel (11\bar{1})_\gamma$ and $[001]_\alpha \parallel [0\bar{1}1]_\gamma$).

(3) The induced phase due to the implantation with 300 keV Fe^+ and Ar^+ ions at room temperature mostly nucleated near the surface. The size and sharp of the induced phase is different depending on ion species. The stress introduced by the concentration gradient of implanted ions has important role to cause the phase transformation, and especially gaseous Ar ions significantly contributes to the phase transformation.

REFERENCES

1) Z. Nishiyama, K. Shimizu, and K. Sugino: Acta Metall. **9** (1961) 620-622.
2) R. P. Reed: Acta Metall. **10** (1962) 865-877.
3) J. Dash and H.M. Otte: Acta Metall. **11** (1963) 1169-1178.
4) R. Lagneborg: Acta metall. **12** (1964) 823-843.
5) H. M. Otte: Acta Metall. **5** (1957) 614-627.
6) B. Cina: Acta Metall. **6** (1958) 748-762.
7) J. A. Venables: Philos. Mag. **7** (1962) 35-44.
8) A. P. Bentley and G. C. smith: Metall. Trans. A **17A** (1986) 1593-1599.
9) P. Rozenak and D. Eliezer: Acta Metall. **35** (1987) 2329-2340.
10) A. Ali, W. A. Grant, and P. J. Grundy: Philos. Mag.B **37** (1978) 353-376.
11) R. M. Boothby and T. M. Williams: J. Nucl. Mat. **96** (1981) 64-70.
12) M. Song, K. Mitsui, M. Takeguchi, K. Furuya, T. Tanabe, and T. Noda: J. Nucl. Mater. **307-311** (2002) 971-975.
13) T. Laursen, J. Whitton, and G. Dearnaley: Mater. Sci. Eng. A**116** (1989) 97-101.
14) S. Raud, H. Garem, A, Naudon, J. P. Villain and P. Moine: Mater. Sci. Eng. **A115** (1989) 245-251.
15) E. Johnson, T. Wohlenberg, and W. A. Grant: Phase Trans. **1** (1979) 23-34.
16) E. Johnson, A. Johansen, L. Sarholt-Kristensen, H. Roy-Poulsen, and A. Christiansen: Nucl. Instrum. Meth. **B7/8** (1985) 212-218.
17) E. Johnson, U. Littmark, and A. Johansen: Philos. Mag. A **45** (1982) 803-821.
18) G. Xie, M. Song, K. Mitsuishi, and K. Furuya: J. Nucl. Mater. **281** (2000) 80-83.
19) E. Johnson, A. Johansen, L. Sarholt-Kristensen, L. Graabaek, N. Hayashi and I. Sakamoto: Nucl. Instrum. Meth. **B19/20** (1987) 171-176.
20) N. Hayashi, E. Johnson, A. Johansen, L. Sarholt-Kristensen and I. Sakamoto: Proc. The International Conference on Martensitic Transformations JIM, Nara-Japan (1986) 539-544.
21) N. Hayashi, I. Sakamoto, and E. Johnson: Proc 12 th Symp. On ISIAT'89 Tokyo (1989) 495-500.
22) A. Johansen, E. Johnson, L. Sarholt-Kristensen, S. Steenstrup, E. Gerrritsen, C.J.M. Denissen, H. Keetels, J. Politiek, N. Hayashi and I. Sakamoto: Nucl. Instrum. Meth. **B50** (1990) 119-126.
23) E. Johnson, A. Johansen, L. Sarholt-Kristensen, L. Graabaek N. Hayashi and I. Sakamoto: Nucl. Instrum. Meth. **B19** (1987) 171-176.
24) E. Johnson, L. Graabaek, A. Johansen, L. Sarholt-Kristensen, P. Borgesen, B.M.U. Scherzer, N. Hayashi and I. Sakamoto: Nucl. Instrum. Meth. **B39** (1989) 567-572.
25) E. Johnson, E. Gerrritsen, N. G. Chechenin, A. Johansen, L. Sarholt-Kristensen, H. A. A. Keetels, L. Graabaek and J. Bohr: Nucl. Instrum. Meth. **B39** (1989) 573-577.
26) J. Noordhuis and J. Th. M. De Hosson: Acta Metall. Mater. **38** No. 11 (1990) 2067-2072.
27) Z. Nishiyama: Sci. Rep. Tohoku Univ. **28** (1934) 627.
28) G. Kurdjumov and G. Sacks: Z. F. Phys. **64** (1930) 325-343.